IRAQI JOURNAL OF MATERIALS
Volume (4) Issue (4) October-December 2025, pp. 179-188

Effects of Nanoparticles Content on Gamma-Ray Shielding Parameters of Magnetite/PDMS Nanocomposites

Munir A. Nafeh

Department of Materials Engineering, Faculty of Engineering, University of Tanta, Egypt

Abstract
This study investigates the gamma ray shielding properties of flexible polydimethylsiloxane (PDMS) nanocomposites loaded with varying concentrations (0–50 wt.%) of magnetite (Fe_3O_4) nanoparticles. The composites were prepared via sonication and tested against gamma-ray energies ranging of 0.103 MeV, 0.662 MeV, 0.826 MeV, and 1.275 MeV. Radiation parameters, including Mass Attenuation Coefficient (MAC), Linear Attenuation Coefficient (LAC), Half-Value Layer (HVL), and Effective Atomic Number (Z_{eff}), were analyzed. Results demonstrated a significant, concentration-dependent improvement in shielding performance across all tested energies. The most dramatic enhancement was observed at the lowest energy (0.103 MeV), where the HVL decreased from ~3.5 cm (pure PDMS) to <0.5 cm (50% Fe_3O_4). This superior low-energy attenuation is attributed to the strong photoelectric effect resulting from the incorporation of high-Z iron. The findings confirm that Fe_3O_4/PDMS nanocomposites are highly effective, tailorable materials for designing advanced radiation shields, particularly against low-energy gamma radiation.

Keywords: Gamma-ray shielding; Magnetite; Nanoparticles; Nanocomposites
Received: 21 June 2025; **Revised:** 29 July 2025; **Accepted:** 5 August 2025; **Published:** 1 October 2025

1. Introduction

Polymer inorganic composites (PINCs) are a class of materials that combine the unique properties of both organic polymers and inorganic fillers to create new materials with enhanced or synergistic functionalities. These composites leverage the desirable attributes of polymers, such as their low density, flexibility, and ease of processing, with the superior properties of inorganic materials, including high strength, thermal stability, and radiation shielding capabilities. The choice of polymer matrix and inorganic filler is critical and tailored to the intended application. Common polymer matrices include poly(dimethylsiloxane) (PDMS), epoxy resins, and polyethylene, while inorganic fillers can be in the form of nanoparticles (Fe_3O_4, ZnO, SiO_2), microparticles ($BaSO_4$, lead oxide), or fibers (glass, carbon).

The advantages of PINCs are numerous and drive their widespread applications. A key benefit is the ability to tune the material properties by controlling the type, size, shape, and concentration of the inorganic filler. For instance, incorporating high atomic number (Z) fillers like Fe_3O_4 can significantly enhance the material's ability to attenuate gamma rays, making it a powerful radiation shield. Other advantages include improved mechanical properties such as increased tensile strength and hardness, enhanced thermal conductivity for heat dissipation, and superior electrical properties for use in capacitors and sensors. The fabrication of PINCs typically involves methods that ensure a homogeneous dispersion of the inorganic phase within the polymer matrix to prevent agglomeration and achieve optimal performance. Common fabrication methods include melt mixing, solution mixing, and in-situ polymerization. In melt mixing, the polymer and filler are blended at an elevated temperature until the filler is uniformly dispersed. Solution mixing involves dissolving the polymer in a solvent, dispersing the filler in the solution, and then removing the solvent to form the composite. In-situ polymerization, often used for nanoparticles, involves synthesizing the polymer in the presence of the nanoparticles, which can lead to excellent dispersion and strong interfacial bonding. These fabrication techniques are chosen based on the properties of the polymer and filler, and the desired final properties of the composite. Due to their customizable properties, PINCs have found diverse applications across various fields. In medicine, they are used for radiation shielding in medical imaging and radiotherapy. In aerospace and defense, they serve as lightweight structural components and thermal management systems. In electronics, they are utilized in dielectric materials, conductive adhesives, and flexible electronics. The versatility and tunability of PINCs make them a cornerstone of modern materials science and engineering.

Magnetite (Fe_3O_4) nanoparticles are a type of iron oxide with unique physical and chemical properties that make them highly valuable in various fields. Physically, they are characterized by their

superparamagnetism at the nanoscale, meaning they only exhibit magnetic properties when an external magnetic field is applied and lose their magnetization when the field is removed. This superparamagnetic behavior prevents agglomeration of the nanoparticles in the absence of a magnetic field, which is crucial for many applications. They also have a large surface area-to-volume ratio, which enhances their chemical reactivity and allows for surface functionalization. Chemically, Fe_3O_4 nanoparticles are relatively stable and possess a high surface energy, which can be harnessed for catalytic activity. Their non-toxic and biocompatible nature makes them suitable for biomedical applications.

The preparation methods and techniques for synthesizing Fe_3O_4 nanoparticles are diverse, each offering control over size, shape, and surface chemistry. The most common method is co-precipitation, where a mixture of ferrous (Fe^{2+}) and ferric (Fe^{3+}) salts is precipitated in an alkaline solution under controlled conditions. This method is simple and cost-effective but can result in a wide size distribution. Another popular technique is thermal decomposition of organometallic precursors in high-boiling point organic solvents, which yields highly crystalline and monodisperse nanoparticles. Hydrothermal synthesis involves a high-temperature and high-pressure aqueous solution to synthesize the nanoparticles, offering precise control over particle morphology. Other methods include the sol-gel method, microemulsion techniques, and sonochemical synthesis, each tailored to specific requirements.

The unique properties and tunable synthesis of Fe_3O_4 nanoparticles lead to a wide range of applications and practical uses. In the biomedical field, they are used for targeted drug delivery, where they can be guided to a specific site in the body using an external magnetic field. They are also employed in magnetic hyperthermia to treat cancer by generating localized heat to destroy tumor cells. Their use as magnetic resonance imaging (MRI) contrast agents enhances the quality of medical images. Beyond medicine, they are used in environmental remediation for removing heavy metals and pollutants from water due to their high adsorption capacity and ease of magnetic separation. In catalysis, they serve as effective catalysts and catalyst supports. Their magnetic properties are also exploited in ferrofluids and in data storage devices. In radiation shielding, their high atomic number and density make them excellent fillers in composites to block gamma rays. The versatility of magnetite nanoparticles, stemming from their unique properties and the ability to control their synthesis, ensures their continued prominence in materials science and technology.

Poly(dimethylsiloxane) (PDMS) is a versatile synthetic polymer belonging to the silicone family, with a chemical formula of $[-Si(CH_3)_2O-]n$. Its backbone consists of a silicon-oxygen chain, which gives it a unique set of physical and chemical properties. Physically, PDMS is an elastomer, meaning it is a soft, viscoelastic material that can be easily deformed and returns to its original shape. It is transparent, optically clear, and highly permeable to gases like oxygen and carbon dioxide, making it suitable for applications requiring gas exchange. Its surface is hydrophobic, repelling water, which is a desirable property in many microfluidic and biomedical devices. Chemically, PDMS is inert and stable over a wide range of temperatures, from approximately −50°C to 200°C. It is resistant to oxidation, UV radiation, and many common chemicals, although it can swell when exposed to non-polar organic solvents.

The advantages of PDMS are numerous. Its low cost, ease of fabrication, and ability to be molded into complex micro- and nanostructures using techniques like soft lithography have made it a cornerstone of microfluidics and lab-on-a-chip technologies. Its transparency and optical properties are beneficial for microscopy and optical sensing. The high gas permeability is critical for cell culture applications, ensuring that cells receive adequate oxygen. Furthermore, its biocompatibility is a major advantage, as it is non-toxic and well-tolerated by biological systems, making it a preferred material for medical implants, drug delivery systems, and tissue engineering scaffolds.

However, PDMS also has some disadvantages. While its hydrophobic nature is often beneficial, it can lead to non-specific protein and biomolecule adsorption, which can interfere with some biological assays. The swelling in organic solvents can limit its use in certain chemical processes. Its relatively low mechanical strength and modulus compared to other engineering plastics can be a limitation for high-stress applications. Additionally, its high gas permeability can be a disadvantage in applications requiring a hermetic seal. Regarding toxicity and biocompatibility, extensive research has shown PDMS to be non-toxic and highly biocompatible. It does not elicit a significant inflammatory response or rejection when implanted in the body. The preparation of PDMS typically involves the mixing of a liquid base monomer with a curing agent, followed by a thermal curing process. The base polymer is a linear chain, while the curing agent, usually a platinum-based catalyst, crosslinks the chains to form a solid, elastic network. The ratio of the base to the curing agent can be adjusted to tune the mechanical properties, such as stiffness and elasticity.

ISSN (print) 2958-8960 (online) 3006-6042 Printed in IRAQ

Applications of PDMS are incredibly diverse. In the biomedical field, it is used for contact lenses, catheters, medical implants, and microfluidic devices for drug screening and diagnostics. In materials science, it is used for soft robotics, flexible electronics, and as a component in various composites. Its use in microfluidics has revolutionized chemical and biological research by enabling high-throughput screening and single-cell analysis. PDMS is also used in consumer products, such as lubricants, sealants, and components in personal care products.

2. Experimental Work

The nanocomposite samples were prepared by manually mixing 5 mL of liquid PDMS ($CH_3[Si(CH_3)_2O]Si(CH_3)_3$) with different weight percentages (wt.%) of magnetite (Fe_3O_4) nanoparticles (0-50%). The mixture was sonicated for 30 minutes to ensure homogeneous distribution of the nanoparticles within the polymer. The mixture was then poured in circular mold and left for 24 hour to solidify in clean environment to avoid the contamination and reaction with the air components. The thickness of the sample was controlled by the volume of the mixture to be constant (2.54 cm). Table (1) shows the specifications of the prepared samples.

Table (1) Specifications of the prepared nanocomposite samples

Sample	Thickness (cm)	PDMS (%)	Fe_3O_4 NPs (%)	Density (g/cm^3)
A1	2.54	100	0	0.965
A2	2.54	95	5	1.006
A3	2.54	90	10	1.050
A4	2.54	85	15	1.099
A5	2.54	80	20	1.152
A6	2.54	75	25	1.211
A7	2.54	70	30	1.276
A8	2.54	65	35	1.348
A9	2.54	60	40	1.429
A10	2.54	55	45	1.521
A11	2.54	50	50	1.625

The prepared nanocomposite samples were tested as shielding materials for gamma rays using 4 different gamma-rays photon energies (0.103 MeV, 0.662 MeV, 0.826 MeV, and 1.275 MeV). These energies were produced by the following radioactive sources Am-241, Cs-137, Co-60, and Na-22, respectively. Figure (1) shows schematically the experimental setup used for the gamma-rays shielding experiments.

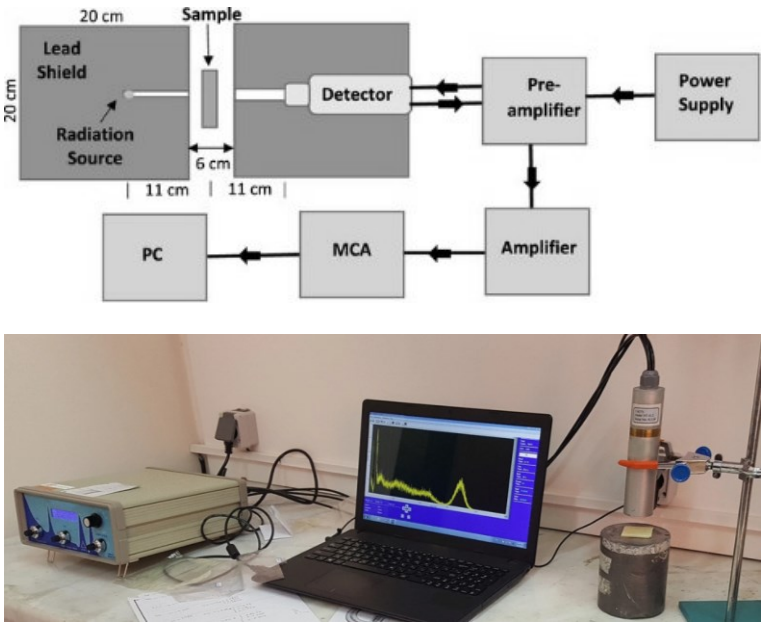

Fig. (1) Schematic diagram and photograph of the experimental setup used for the gamma-rays shielding experiments

3. Results and Discussion

Figure (2) illustrates the relationship between the mass attenuation coefficient (MAC) of iron oxide (Fe_3O_4) nanoparticles (NPs)/PDMS nanocomposites and the weight percentage of the Fe_3O_4 NPs, at various gamma ray energies. The MAC is a measure of how effectively a material absorbs or scatters radiation. It depends on the material's composition and the energy of the incident radiation. This figure shows four distinct curves, each corresponding to a specific gamma ray energy: 0.103 MeV (blue), 0.662 MeV (red), 0.826 MeV (black), and 1.606 MeV (green). The x-axis represents the weight percentage of Fe_3O_4 NPs in the nanocomposite, ranging from 0% (pure PDMS) to 50%. The y-axis shows the MAC in cm2/g. The data reveals a significant dependency of the nanocomposite's radiation shielding properties on both the concentration of Fe_3O_4 NPs and the energy of the gamma rays.

The most striking feature of the graph is the dramatic increase in MAC for the lowest energy gamma rays (0.103 MeV) as the concentration of Fe_3O_4 NPs increases. This behavior is consistent with the photoelectric effect, which is the dominant interaction mechanism for low-energy photons and materials with high atomic numbers. Fe_3O_4 contains iron (Z=26), which has a much higher atomic number than the elements in PDMS (polydimethylsiloxane) like silicon (Z=14), carbon (Z=6), and oxygen (Z=8). As the concentration of high-Z material (Fe_3O_4) increases, the probability of the photoelectric effect rises, leading to a much higher MAC. In contrast, for the higher gamma ray energies (0.662 MeV, 0.826 MeV, and 1.606 MeV), the MAC shows only a slight increase with the concentration of Fe_3O_4 NPs. At these higher energies, the dominant interaction mechanisms are Compton scattering and pair production. Compton scattering, which is the scattering of a photon by an electron, is less dependent on the atomic number of the material than the photoelectric effect. Pair production requires a photon energy greater than 1.022 MeV and its probability increases with the atomic number squared (Z^2). However, at these energies, the total MAC is much lower compared to the low energy range. The data clearly demonstrates the superior shielding capability of the Fe_3O_4/PDMS nanocomposites for low-energy gamma rays, making them highly effective for applications where low-energy radiation is a concern. The slight increase in MAC at higher energies still highlights the contribution of the high-Z filler in improving the shielding properties. This study underscores the importance of tailoring the material composition to the specific energy range of the radiation to be shielded.

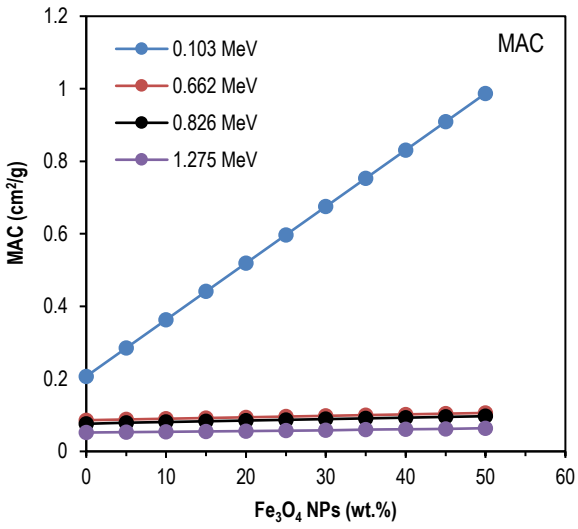

Fig. (2) Variation of MAC with the weight percentage of Fe_3O_4 NPs in the prepared nanocomposites

Figure (3) shows the linear attenuation coefficient (LAC) as a function of the weight percentage of Fe_3O_4 nanoparticles (NPs) in Fe_3O_4 NPs/PDMS nanocomposites, for various gamma ray energies. The LAC is a measure of how effectively a material reduces the intensity of a beam of radiation as it passes through. Unlike the mass attenuation coefficient (MAC), which is independent of the material's density, the LAC is density-dependent. This means that as the concentration of the denser Fe_3O_4 NPs increases, the overall density of the nanocomposite also increases, contributing to a higher LAC. This figure displays four curves, each representing a different gamma ray energy: 0.103 MeV (blue), 0.662 MeV (red), 0.826 MeV (black), and 1.606 MeV (green). The x-axis indicates the weight percentage of Fe_3O_4 NPs (0% to 50%), while the y-axis shows the LAC in cm^{-1}. The graph reveals a clear correlation between

ISSN (print) 2958-8960 (online) 3006-6042 Printed in IRAQ

the nanocomposite's radiation shielding efficacy, the concentration of Fe_3O_4 NPs, and the energy of the incident gamma rays.

The most prominent trend in the graph is the sharp, non-linear increase in the LAC for the lowest energy gamma rays (0.103 MeV) as the concentration of Fe_3O_4 NPs rises. This significant enhancement in attenuation is primarily due to the photoelectric effect, which is the dominant interaction for low-energy photons with materials composed of high atomic number (Z) elements. Since iron (Z=26) has a much higher Z than the elements in PDMS, increasing the Fe_3O_4 content substantially boosts the photoelectric absorption probability, leading to a massive increase in the LAC. The non-linear nature of this increase suggests a more complex relationship than a simple linear combination, likely due to the changing density and the synergistic effects of the composite. In contrast, for the higher gamma ray energies (0.662 MeV, 0.826 MeV, and 1.606 MeV), the LAC shows only a marginal, nearly linear increase with the Fe_3O_4 concentration. At these energies, Compton scattering is the primary interaction mechanism, which is less sensitive to the atomic number of the material. While the increase in Fe_3O_4 content does raise the LAC, the effect is far less pronounced compared to the low-energy range. This behavior confirms the high-Z material's superior shielding performance against low-energy gamma rays and its more moderate, but still positive, contribution to shielding at higher energies. The figure also highlights the potential of using Fe_3O_4/PDMS nanocomposites as effective radiation shields, especially for applications involving low-energy gamma radiation, by simply adjusting the concentration of the Fe_3O_4 NPs.

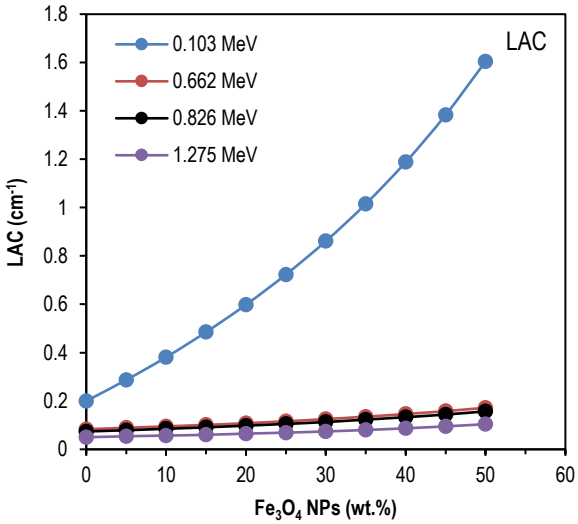

Fig. (3) Variation of LAC with the weight percentage of Fe_3O_4 NPs in the prepared nanocomposites

Figure (4) depicts the relationship between the half-value layer (HVL) and the weight percentage of Fe_3O_4 nanoparticles (NPs) in Fe_3O_4 NPs/PDMS nanocomposites, at various gamma ray energies. The HVL is the thickness of a material required to reduce the intensity of an incident radiation beam to half of its original value. It's an inverse measure of a material's shielding effectiveness; a smaller HVL indicates a more effective shield. The HVL is inversely proportional to the linear attenuation coefficient (LAC), meaning a higher LAC leads to a smaller HVL. This figure features four distinct curves, each representing a different gamma ray energy: 0.103 MeV (blue), 0.662 MeV (red), 0.826 MeV (black), and 1.606 MeV (green). The x-axis shows the weight percentage of Fe_3O_4 NPs, ranging from 0% (pure PDMS) to 50%. The y-axis represents the HVL in cm. The data clearly shows that the nanocomposite's shielding performance is a function of both the concentration of the Fe_3O_4 NPs and the energy of the incident gamma rays.

The most significant trend is the substantial decrease in the HVL for all gamma ray energies as the weight percentage of Fe_3O_4 NPs increases. This decrease signifies a direct improvement in the radiation shielding capability of the nanocomposite. The most dramatic reduction in HVL occurs for the lowest energy gamma rays (0.103 MeV), with the HVL dropping from approximately 3.5 cm for pure PDMS to less than 0.5 cm for a 50% Fe_3O_4 concentration. This is due to the strong photoelectric effect at low energies, which is highly dependent on the atomic number (Z) of the material. As the concentration of high-Z iron (Z=26) in the composite increases, photoelectric absorption becomes the dominant

ISSN (print) 2958-8960 (online) 3006-6042 Printed in IRAQ

interaction, significantly enhancing the shielding. For the higher energies (0.662 MeV, 0.826 MeV, and 1.606 MeV), the HVL also decreases with increasing Fe_3O_4 content, but the reduction is less pronounced. This is because at higher energies, Compton scattering is the primary interaction mechanism. While the presence of high-Z iron contributes to scattering, the effect is not as strong as the photoelectric effect. This data confirms that incorporating high-Z materials like Fe_3O_4 into a polymer matrix like PDMS is an effective strategy for developing efficient radiation shields. Figure (4) also provides crucial quantitative data for designing and optimizing nanocomposite shields for specific applications and energy ranges, demonstrating that a higher concentration of Fe_3O_4 NPs consistently leads to better shielding, particularly for low-energy gamma radiation.

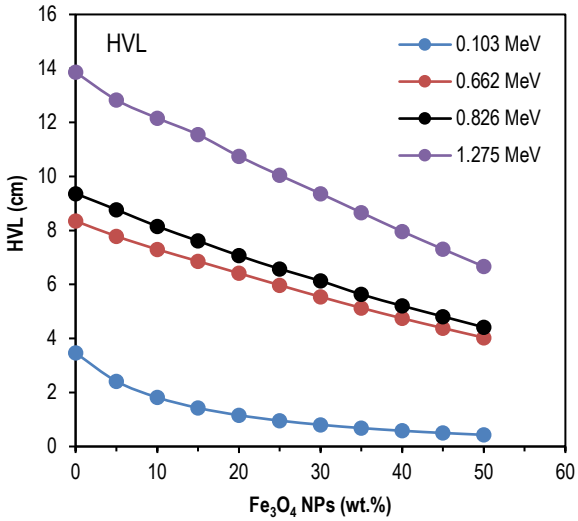

Fig. (4) Variation of HVL with the weight percentage of Fe_3O_4 NPs in the prepared nanocomposites

Figure (5) illustrates the relationship between the tenth-value layer (TVL) and the weight percentage of Fe_3O_4 nanoparticles (NPs) in Fe_3O_4 NPs/PDMS nanocomposites, for various gamma ray energies. The TVL is the thickness of a material required to reduce the intensity of an incident radiation beam to one-tenth of its original value. It's a key parameter in radiation shielding, directly indicating a material's effectiveness; a smaller TVL means a more efficient shield. The TVL is related to the half-value layer (HVL) and the linear attenuation coefficient (LAC) by the equations TVL=HVL/0.301 and TVL=2.303/LAC, respectively. This figure shows four distinct curves, each corresponding to a specific gamma ray energy: 0.103 MeV (blue), 0.662 MeV (red), 0.826 MeV (black), and 1.606 MeV (green). The x-axis represents the weight percentage of Fe_3O_4 NPs (0% to 50%), while the y-axis shows the TVL in cm. The data highlights a strong dependency of the nanocomposite's shielding effectiveness on both the concentration of the high-Z filler and the energy of the gamma rays.

The most prominent trend is the consistent decrease in the TVL for all gamma ray energies as the weight percentage of Fe_3O_4 NPs increases. This decrease signifies a direct improvement in the radiation shielding capability of the nanocomposite. The most dramatic reduction in TVL occurs for the lowest energy gamma rays (0.103 MeV), with the TVL dropping sharply from approximately 11.5 cm for pure PDMS to just over 1 cm for a 50% Fe3O4 concentration. This is primarily due to the photoelectric effect, which dominates low-energy photon interactions and is highly sensitive to the atomic number (Z) of the absorbing material. The presence of high-Z iron (Z=26) greatly enhances this effect, making the material a much more effective shield at this energy. For the higher energies (0.662 MeV, 0.826 MeV, and 1.606 MeV), the TVL also decreases with increasing Fe_3O_4 content, but the reduction is less steep. At these energies, Compton scattering is the main interaction mechanism. While adding a higher-Z material still improves shielding, its effect is not as pronounced as in the photoelectric regime. The figure also provides quantitative evidence that incorporating high-Z materials like Fe_3O_4 into a polymer matrix is an effective strategy for developing highly efficient radiation shields. It also allows for the precise selection of a composite's composition to achieve a desired shielding level for a specific gamma ray energy, making this a valuable tool for designing protective materials.

ISSN (print) 2958-8960 (online) 3006-6042 Printed in IRAQ

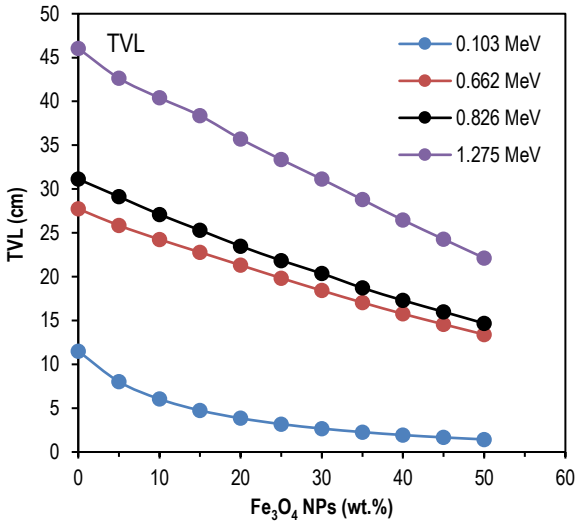

Fig. (5) Variation of TVL with the weight percentage of Fe_3O_4 NPs in the prepared nanocomposites

Figure (6) shows the relationship between the mean free path (MFP) and the weight percentage of Fe_3O_4 nanoparticles (NPs) in Fe_3O_4 NPs/PDMS nanocomposites, for various gamma ray energies. The MFP is the average distance a gamma ray travels in a material before it undergoes an interaction (e.g., absorption or scattering). It is a measure of the material's transparency to radiation; a longer MFP means the material is less effective at shielding. The MFP is inversely proportional to the linear attenuation coefficient (LAC). This figure features four curves, each corresponding to a different gamma ray energy: 0.103 MeV (blue), 0.662 MeV (red), 0.826 MeV (black), and 1.606 MeV (green). The x-axis represents the weight percentage of Fe_3O_4 NPs, ranging from 0% (pure PDMS) to 50%. The y-axis shows the MFP in cm. The data clearly indicates that the nanocomposite's radiation shielding performance is a function of both the concentration of the Fe_3O_4 NPs and the energy of the incident gamma rays.

The most prominent feature of the graph is the consistent decrease in the MFP for all gamma ray energies as the weight percentage of Fe_3O_4 NPs increases. This decrease signifies that the gamma rays are traveling a shorter average distance before interacting, which directly corresponds to an improvement in the material's shielding effectiveness. The most dramatic reduction in MFP occurs for the lowest energy gamma rays (0.103 MeV). For pure PDMS, the MFP is approximately 5 cm, but for a 50% Fe_3O_4 concentration, it drops to less than 1 cm. This sharp decline is primarily due to the photoelectric effect, which is the dominant interaction for low-energy photons and is highly dependent on the atomic number (Z) of the material. By increasing the concentration of high-Z iron (Z=26), the probability of photoelectric absorption increases significantly, leading to a much shorter MFP. In contrast, for the higher energies (0.662 MeV, 0.826 MeV, and 1.606 MeV), the MFP also decreases with increasing Fe_3O_4 content, but the reduction is less steep. At these higher energies, Compton scattering is the main interaction mechanism. While adding a higher-Z material still improves shielding by increasing the scattering probability, the effect is not as pronounced as in the photoelectric regime. This figure also provides crucial quantitative data for designing and optimizing nanocomposite shields for specific applications and energy ranges, demonstrating that a higher concentration of Fe_3O_4 NPs consistently leads to better shielding, especially for low-energy gamma radiation.

Figure (7) illustrates the relationship between the effective atomic number (Z_{eff}) and the weight percentage of Fe_3O_4 nanoparticles (NPs) in Fe_3O_4 NPs/PDMS nanocomposites, for various gamma ray energies. The Z_{eff} is a weighted average of the atomic numbers of the elements in a composite material. It's a crucial parameter in radiation physics as it provides insight into how a composite material will interact with radiation. A higher Z_{eff} generally means better shielding properties, particularly at low energies. This figure shows four distinct curves, each representing a different gamma ray energy: 0.103 MeV (blue), 0.662 MeV (red), 0.826 MeV (black), and 1.606 MeV (green). The x-axis represents the weight percentage of Fe_3O_4 NPs, ranging from 0% (pure PDMS) to 50%. The y-axis shows the Z_{eff}. The data reveals a significant dependency of the nanocomposite's radiation shielding properties on both the concentration of Fe_3O_4 NPs and the energy of the incident gamma rays.

The most notable feature of the graph is the consistent increase in the Z_{eff} for all gamma ray energies as the weight percentage of Fe_3O_4 NPs increases. This is an expected result, as adding a high-Z material

like iron (Z=26) to a low-Z matrix like PDMS (composed of Si, C, and O, with Zs of 14, 6, and 8, respectively) will naturally raise the overall effective atomic number of the composite. However, the magnitude of this increase is highly dependent on the energy of the gamma rays. The most dramatic increase in Z_{eff} is seen at the lowest energy (0.103 MeV), where the Z_{eff} rises from about 6.5 (for pure PDMS) to over 22 at a 50% Fe_3O_4 concentration. This is because at low energies, the dominant interaction is the photoelectric effect, whose cross-section is proportional to Zn, where 'n' can be as high as 4 or 5. This strong dependence on Z makes the effective Z calculation sensitive to the high-Z component. As the energy increases, the Z_{eff} curves flatten out, and the overall Z_{eff} values decrease for a given Fe_3O_4 concentration. At higher energies, the dominant interaction is Compton scattering, which is less dependent on the atomic number. This makes the effective Z calculation less sensitive to the high-Z material and more reflective of the average electron density of the composite. Figure (7) provides valuable insight into how the addition of a high-Z material can be used to engineer a nanocomposite with a tailored effective atomic number, allowing for the optimization of its shielding properties for specific radiation energy ranges.

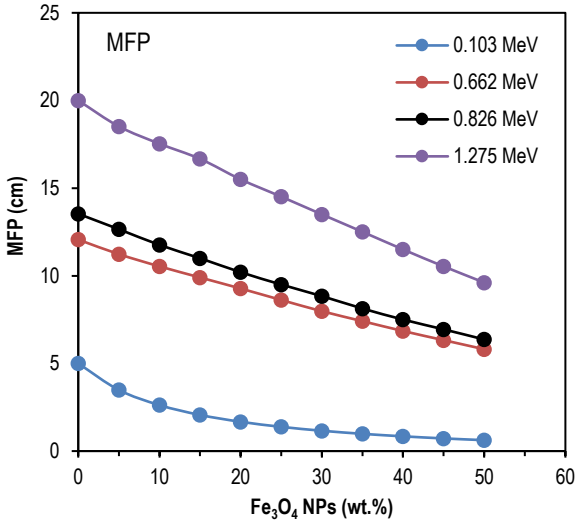

Fig. (6) Variation of MFP with the weight percentage of Fe_3O_4 NPs in the prepared nanocomposites

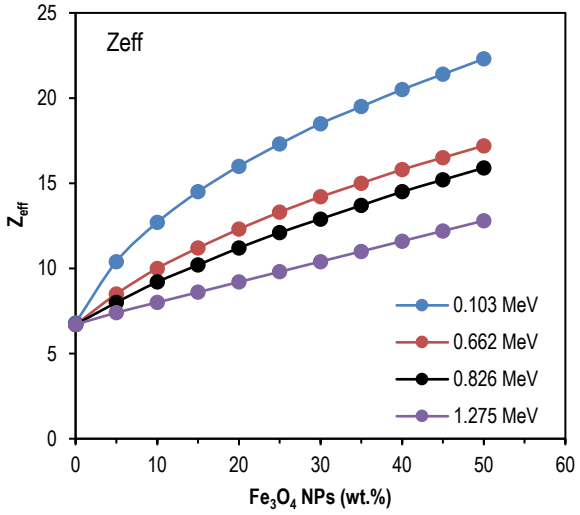

Fig. (7) Variation of Zeff with the weight percentage of Fe_3O_4 NPs in the prepared nanocomposites

4. Conclusion

Incorporating Fe_3O_4 nanoparticles into the PDMS matrix significantly enhances the gamma radiation shielding capabilities. The high-Z iron component causes a dramatic improvement in the MAC, LAC,

ISSN (print) 2958-8960 (online) 3006-6042 Printed in IRAQ

and Z_{eff}, while concurrently reducing the HVL, TVL, and MFP. This effect is most prominent at low gamma ray energies (0.103 MeV), where the photoelectric effect is the dominant interaction mechanism. At higher energies, the shielding is still improved, though less steeply, due to Compton scattering. The results confirm that Fe_3O_4/PDMS nanocomposites are effective, tunable radiation shields, particularly for low-energy applications, by optimizing the Fe_3O_4 concentration.

References

[1] Z. Li et al., "Sonochemical fabrication of inorganic nanoparticles for applications in catalysis", *Ultrason. Sonochem.*, 71 (2021) 105384.
[2] A. Hosseinkhani, M. Omidkhah and A.E. Amooghin, "Fine-tuning CO_2 separation of mixed matrix membranes by constructing efficient transport pathways through the addition of hybrid porous 2D nanosheets", *Chem. Eng. J. Adv.*, 20 (2024) 100685.
[3] Z. Bai and B. Zhang, "Fabrication of superhydrophobic reduced-graphene oxide/nickel coating with mechanical durability, self-cleaning and anticorrosion performance", *Nano Mater. Sci.*, 2(2) (2020) 151-158.
[4] J. Chang et al., "Ultra-thin metal composites for electromagnetic interference shielding", *Compos. B: Eng.*, 246 (2022) 110269.
[5] M. Abu Elezz et al., "A comprehensive review: Functional nanomaterials for renewable energy: Innovations, applications, and sustainable strategies", *Next Mater.*, 9 (2025) 101001.
[6] R.M. Obaid, A.Al-Jawdah, and R.M. Aljarrah, "Evaluation of the Capability of Utilizing the Local Soil as a Nuclear Radiation Shielding Materials", *Iraqi J. Appl. Phys.*, 21(2) (2025) 205-208.
[7] H. Gao et al., "Recent advancements in electro-thermal anti-/de-icing materials", *RSC Adv.*, 15(22) (2025) 17102-17115.
[8] R.X.Z. Lu and M. Radisic, "Organ-on-a-chip platforms for evaluation of environmental nanoparticle toxicity", *Bioactive Mater.*, 6(9) (2021) 2801-2819.
[9] H. Wei et al., "Intermetallic compounds for nitrogen electrochemistry", *Green Energy Enviro.*, 10(2) (2025) 268-291.
[10] K.K. Lee et al., "Self-assembled multicolor fluorescent nanoparticles derived from dopamine analogues: A versatile platform for biomedical applications", *Chem. Eng. J.*, 495 (2024) 152739.
[11] D.K. Chandra, A. Kumar and C. Mahapatra, "Smart nano-hybrid metal-organic frameworks: Revolutionizing advancements, applications, and challenges in biomedical therapeutics and diagnostics", *Hybrid Adv.*, 9 (2025) 100406.
[12] S. Liu et al., "Rational design of metal–organic framework-nanoparticle composite electrocatalysts for sustainable nitrogen electrochemistry", *eScience*, (2025) 100378.
[13] N. Zhang et al., "Supramolecular self-assembly of nickel (Ⅱ)-substituted α-Keggin-type polyoxometalate and polyaniline coated Fe_2O_3 hollow nanospindle for microwave absorption application", *Prog. Nat. Sci.: Mater. Int.*, 31(3) (2021) 387-397.
[14] Y.X. Gan, "Recent development of thermoelectric nanofibers and their composites", *J. Materiomics*, 9(1) (2023) 99-130.
[15] S.K. Ghadei, K.J. Sankaran and R. Sakthivel, "Hybrid nano-interfacial engineering of special-wettable surfaces for advanced oil/water separation: Multifunctional strategies and future directions", *Results Surf. Interfaces*, 19 (2025) 100526.
[16] R. Fitaihi et al., "Safety and Efficacy of Dissolvable Microneedles Embedded with Dexamethasone-Loaded Nanoparticles for Treating Ocular Inflammation", *Int. J. Pharmaceut.*, 681 (2025) 125871.
[17] L.A. Hamza and S.H. Al-nesrawy, "Influence of Ferrite Nanoparticles Addition on Structural and Dielectric Properties of PS/PMMA Blend for Gamma Shielding Application", *Iraqi J. Appl. Phys.*, 21(4) (2025) 514-519.
[18] B. Salah et al., "Unveiling the electrochemical CO oxidation activity on support-free porous PdM (M = Fe, Co, Ni) foam-like nanocrystals over a wide pH range", *Energy Conv. Manage.: X*, 20 (2023) 100449.
[19] N.F. Pikau et al., "Gamma alumina as a saturable absorbing material for C- and L-band ultrafast mode-locked fiber lasers", *Results Phys.*, 61 (2024) 107759.
[20] A.S. Embaye et al., "High-performance antifouling photothermal membranes for enhanced membrane distillation crystallization", *Desalin.*, 608 (2025) 118847.
[21] M. Aliofkhazraei et al., "Review of plasma electrolytic oxidation of titanium substrates: Mechanism, properties, applications and limitations", *Appl. Surf. Sci. Adv.*, 5 (2021) 100121.
[22] A. Yazdanpanah et al., "Passivity and breakdown mechanisms in laser powder bed fusion processed Ni-based Alloy 625: Influence of scan strategy", *Corros. Sci.*, 255 (2025) 113129.
[23] B.K. Dejene and A.Y. Melese, "Textile-Based Triboelectric Nanogenerators: A Critical Review of Materials, Fabric Designs, and Washability for Wearable Applications", *J. Sci.: Adv. Mater. Dev.*, (2025) 100975.
[24] Y. Liu et al., "Derivation of carbonaceous nanoparticles from glucose-modified nickel-titanium oxide nanoparticles grown on Nitinol fiber for solid phase microextraction of several polycyclic aromatic hydrocarbons in water samples", *Talanta Open*, 3 (2021) 100030.
[25] W.K. Abood and Z.J. Raheem, "Calculation of Mass Attenuation Coefficients and Cross Sections for Different Elemental Metals", *Iraqi J. Appl. Phys. Lett.*, 7(2) (2024) 15-18.
[26] C.B. Adamo, R.J. Poppi, and D.P. de Jesus, "Improving surface-enhanced Raman scattering performance of gold-modified magnetic nanoparticles by using nickel-phosphorus film on polydimethylsiloxane", *Microchem. J.*, 160(B) (2021) 105704.
[27] Z.U. Zango et al., "A state-of-the-art review on green synthesis and modifications of ZnO nanoparticles for organic pollutants decomposition and CO_2 conversion", *J. Hazard. Mater. Adv.*, 17 (2025) 100588.
[28] Y. Ma et al., "Transformation gap from research findings to large-scale commercialized products in microfluidic field", *Mater. Today Bio*, 29 (2024) 101373.
[29] M. Pourmohammad, A. Ghadi and A.A. Beni, "Response surface methodology for adsorption of propylparaben using zeolitic imidazolate-67 modified by Fe_3O_4 nanoparticles from aqueous solutions", *Desalin. Water Treat.*, 304 (2023) 169-180.
[30] A. Al Rashid et al., "Cobalt iron oxide ($CoFe_2O_4$) reinforced polyvinyl alcohol (PVA) based magnetoactive polymer nanocomposites for remote actuation", *Mater. Sci. Eng. B*, 311 (2025) 117838.
[31] Y. Ma et al., "Renewable saccharide-derived porous carbon foams with metal particles for CNT and graphene substrates in electrochemical applications", *iScience*, 28(3) (2025) 112050.
[32] U.V. Romero et al., "A biocompatible nitinol based triboelectric stent sensor for prospective cardiovascular health monitoring", *Hybrid Adv.*, 10 (2025) 100484.
[33] G. Nunziata, A. Borroni and F. Rossi, "Advanced microfluidic strategies for core-shell nanoparticles: the next-generation of polymeric and lipid-based drug nanocarriers", *Chem. Eng. J. Adv.*, 22 (2025) 100759.

[34] I. Hossain et al., "Structural, morphological, optical and electrical properties of ferrite-based nanoparticles synthesized flexible substrate for chemical sensing application", *J. Sci.: Adv. Mater. Dev.*, 9(3) (2024) 100750.
[35] W.K. Abood, Z.J. Raheem, and R.R. Mohammed, "Determination of Mass Attenuation Coefficient of PVC and Iron Oxide (Fe_2O_3) Alloy", *Iraqi J. Appl. Phys. Lett.*, 8(3) (2025) 79-81.
[36] M.S. Hareesh, P. Joseph and S. George, "Electromagnetic interference shielding: a comprehensive review of materials, mechanisms, and applications", *Nanoscale Adv.*, 7(15) (2025) 4510-4534.
[37] F. Belén, J. Gutiérrez and V. Springer, "Recent advances in environmental sample preparation: Nanomaterials, automation, and sustainable strategies", *Adv. Sample Preparation*, 14 (2025) 100171.
[38] S. Puri et al., "A review on bio-inspired nanoparticles and their impact on membrane applications", *RSC Sustain.*, 3(3) (2024) 1212-1233.
[39] M. Jois, A. Gebrekrstos and A. Elias, "Mechanical Rolling of Nickel Nanowire-PVDF Composites Yields Enhanced Conductivity and Electromagnetic Shielding Properties", *Results Eng.*, (2025) 106699.
[40] W. Zhao et al., "Combining printing and nanoparticle assembly: Methodology and application of nanoparticle patterning", *The Innovation*, 3(4) (2022) 100253.
[41] I. Ozcicek, "A critical review of in vitro and in vivo biomedical applications of gold nanoparticles: From toxicology to cancer therapy", *Biomed. Pharmaco.*, 190 (2025) 118410.
[42] D. Sharma and S. Bose, "The journey of PDMS-based nanocomposites for EMI shielding applications: from bench to translational research", *Mater. Adv.*, 2(17) (2021) 5580-5592.
[43] V. Dhand et al., "Synthesis, characterization, and feasibility investigation of dysprosium-doped samarium iron oxide nano-powder/polydimethylsiloxane (Dy-SmFeO/PDMS) nano-composite for dynamic magneto-mechanical stability", *Polym. Test.*, 127 (2023) 108202.
[44] M. Dai et al., "Lightweight flexible Ni@wood ultrathin wood-based superhydrophobic composite film for absorption-dominated electromagnetic interference shielding and electrothermal management", *Indust. Crops Products*, 233 (2025) 121457.

 ISSN (print) 2958-8960 (online) 3006-6042 Printed in IRAQ